JOURNAL OF MATERIALS SCIENCE 26 (1991) 655–660

Interfacial shear stress in SiC fibre-reinforced cordierite

L. R. DHARANI, M. N. RAHAMAN*, S-H. WANG‡
*Department of Mechanical and Aerospace Engineering and Engineering Mechanics, and *Department of Ceramic Engineering, University of Missouri-Rolla, Rolla, Missouri 65401, USA*

An analytical model based on a consistent shear-lag theory was developed to predict the interfacial shear stress in single fibre pull-out tests. The calculations show that the stress is highly dependent on the specimen thickness and the method of testing. Data for the debond stress and the interfacial shear stress were measured for single SiC fibres embedded in a magnesium aluminium silicate (cordierite) matrix. The effect of fibre embedded length, processing schedule, and matrix toughening were investigated. For a fixed sample support configuration during testing, good agreement was obtained between the model predictions and experimental data.

1. Introduction

In fibre-reinforced materials, the interfacial bonding between fibre and matrix can have a significant effect on the physical and mechanical properties of the composite. For ceramic matrix composites in which both the fibres and the matrix are brittle, debonding between the fibres and the matrix and subsequent fibre pull-out may make an important contribution to increasing the fracture toughness. The interfacial shear strength may therefore play a critically important role in determining the fracture toughness of ceramic matrix composites. Relatively low interfacial shear strength is believed to be required for promoting the toughening mechanisms and for reducing the level of brittle failure of the fibres.

The realization of the importance of the fibre–matrix interface for developing the mechanical properties of ceramic matrix composites has led to a growing need for test methods that will allow quantitative characterization of the interface. The single fibre pull-out test provides one of the most direct methods of measuring interface parameters and has been used extensively for polymer and metal matrix composites [1–7]. For a variety of reasons, including the difficulties in fabricating single fibre pull-out samples and scatter in experimental data, it has not been used for ceramic matrix composites until recently [8–11]. Instead less direct tests, e.g. measurement of matrix crack spacing and crack opening displacements during loading and unloading of composites [12] or indentation methods [13, 14] have been used.

Relatively little theoretical work has been done on the shear stresses developed during fibre pull-out [1, 2]. In this study, an analytical model based on a consistent shear-lag theory was developed to predict the interfacial stresses and how these depend on the fibre embedded length and the sample support configuration during testing. In order to test the model, the stress required to cause debonding of the fibre and subsequent pull-out was measured for single SiC fibres embedded in a magnesium aluminium silicate (cordierite) matrix. The effect of fibre embedded length, sample fabrication conditions (time or temperature) and matrix toughening by the incorporation of SiC whiskers were investigated.

2. Theory

The model for predicting the interfacial stresses as a function of the displacement in the fibre pull-out test is based on a consistent shear-lag theory. The idealized geometry of the single fibre pull-out sample considered in the model is shown in Fig. 1. The composite region is divided into a number of vertical elements $(1, 2, \ldots, n, \ldots, N)$ of arbitrary width, h. Then the transverse (x) and axial (y) equilibrium equations for a generic element (n) and the free edge elements (1 and N) are written down as

$$\sigma_{x(n+1/2)} - \sigma_{x(n-1/2)} + (h/2)[\tau_{(n+1/2),y} + \tau_{(n-1/2),y}] + \delta[\sigma_{x(n-1/2)} - (h/2)\tau_{(n-1/2),y}] - \delta_{nN}[\sigma_{x(n+1/2)} + (h/2)\tau_{(n+1/2),y}] = 0 \quad (1)$$

$$\tau_{(n+1/2)} - \tau_{(n-1/2)} + h\sigma_{yn,y} + \delta_{n1}\tau_{(n-1/2)} - \delta_{nN}\tau_{(n+1/2)} = 0 \quad n = 1, 2, \ldots, N \quad (2)$$

where σ_x, σ_y and τ are the transverse normal, axial, and shear stresses, respectively, the subscripts $(n + 1/2)$ and $(n - 1/2)$ indicate the mid-nodes between the elements n and $(n + 1)$, and $(n - 1)$ and n, respectively, subscript y preceded by a comma indicates differentiation with respect to y, and δ_{mn} is the

‡*Permanent address*: Shandong Institute of Industrial Ceramics, Shandong, People's Republic of China.

0022–2461/91 $03.00 + .12 © *1991 Chapman and Hall Ltd.*

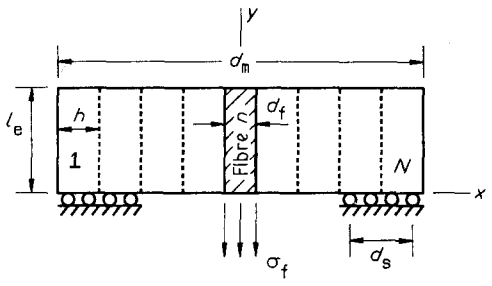

Figure 1 Schematic drawing of the fibre pull-out test geometry used in the analytical model.

Kronecker delta ($\delta_{mn} = 0$ for $m \neq n$ and $\delta_{mn} = 1$ for $m = n$).

In order to make the problem mathematically tractable, a set of approximate constitutive relations were derived based on a consistent shear-lag theory and finite difference approximations [15, 16]. With these approximations the constitutive relations for element n can be written as

$$\sigma_{x(n+1/2)} = \frac{1}{2h}(C_{11}^n + C_{11}^{n+1})(u_{n+1} - u_n) + \frac{1}{2}(C_{12}^n + C_{12}^{n+1})v_{(n+1/2)y} \quad (3)$$

$$\sigma_{y(n)} = C_{12}^n(u_{n+1/2} - u_{n-1/2})/h + C_{22}^n v_{ny} \quad (4)$$

$$\tau_{n+1/2} = \tfrac{1}{2}(C_{66}^n + C_{66}^{n+1})[u_{(n+1/2)y} + (v_{n+1} - v_n)/h] \quad (5)$$

where C_{ij}^n are the elements of the stiffness matrix of element n. The transverse and shear stresses at $(n - 1/2)$ can be obtained by substituting $(n - 1)$ for n in Equations 3 to 5. When these approximate stress–displacement relations are substituted into Equations 1 and 2 the resulting equations in terms of axial and transverse displacements can be written in the following matrix form

$$\{w'\} = [K_w]\{w\} \quad (6)$$

where

$$\{w\} = \{u_1, \ldots, u_N, v_1, \ldots, v_N, u'_1, \ldots, u'_N, \ldots, v'_1, \ldots, v'_N \ldots\}^T \quad (7)$$

and

$$[K_w] = \begin{bmatrix} [0] & [0] & [1] & [0] \\ [0] & [0] & [0] & [1] \\ [K_u] & [0] & [0] & [C_u] \\ [0] & [K_v] & [C_v] & [0] \end{bmatrix}$$

when u_n and v_n representing the x and y displacement components of an element n, the tri-diagonal $(N \times N)$ matrices $[K_u]$, $[K_v]$, $[C_u]$, and $[C_v]$ are functions of the element orthotropic stiffnesses, (C_{ij}), and the element width, h [16], and the primes represent differentiation with respect to the non-dimensional variable, η $(= y/h)$.

The general solution of the equations given above can be written down if the eigenvalues and eigenvectors of the matrix $[K_w]$ are known. Let r_j (with $j = 1, 2, \ldots, K_1$) be the real eigenvalues of the matrix $[K_w]$, $\{A_j\}$ and $\{B_j\}$ be the first $2N$ components of the corresponding eigenvectors, and $p_j + iq_j$ (with p_j, $q_j > 0$, and $j = 1, 2, \ldots, K_2$) be the complex eigenvalues of the matrix $[K_w]$, $\{A_j^R\} + i\{A_j^I\}$ and $\{B_j^R\} + i\{B_j^I\}$ be the first $2N$ components of the corresponding eigenvectors, where K_1 and K_2 are the number of the real and complex eigenvalues, respectively, so that $K_1 + 2K_2 = 4N$. The eigenvalues can be calculated numerically once the matrix $[K_w]$ is formed. Then the general solution to Equations 3 to 5 can be written as

$$\{u\} = \sum_{j=1}^{k_1} C_j\{A_j\}e^{r_j\eta} + \sum_{j=1}^{k_2} e^{p_j\eta}\{C_j^1(\{A_j^R\}\cos q_j\eta - \{A_j^I\}\sin q_j\eta) + C_j^2(\{A_j^R\}\sin q_j\eta + \{A_j^I\}\cos q_j\eta)] \quad (8)$$

$$\{v\} = \sum_{j=1}^{k_1} C_j\{B_j\}e^{r_j\eta} + \sum_{j=1}^{k_2} e^{p_j\eta}\{C_j^1(\{B_j^R\}\cos q_j\eta - \{B_j^I\}\sin q_j\eta) + C_j^2(\{B_j^R\}\sin q_j\eta + \{B_j^I\}\cos q_j\eta)] \quad (9)$$

where C_j, C_j^1, C_j^2 are constants to be determined from the boundary conditions.

3. Experimental procedure

Samples of cordierite containing single fibres of SiC were fabricated by conventional sintering or hot pressing. The fibres (SCS-6; Avco Specialty Materials, Lowell, Massachusetts, USA) had a diameter of ≈ 140 μm and had a carbon core and a non-stoichiometric, carbon-rich layer on the outer surface (Fig. 2). The cordierite matrix powder (with a stoichiometric composition corresponding to $2MgO \cdot 2Al_2O_3 \cdot 5SiO_2$) was prepared in the laboratory by a sol–gel process. The properties of the fibre and matrix assumed in the theoretical analysis are given in Table I.

The samples fabricated by conventional sintering were formed by a slip casting process as shown schematically in Fig. 3. After drying, the samples were sintered in air at 950 °C for 2.5 h. In addition, some samples were heated further at 1050 °C for 2 h in order to examine the effect of oxidation. The fabricated samples were ≈ 8 mm diameter and their thickness varied from 2 to 4 mm.

The method used for fabricating the hot-pressed samples is shown schematically in Fig. 4. A special

TABLE I Fibre and matrix properties used in the analytical model

	Fibre*	Matrix [17]
Density (Mg m^{-3})	3.2	2.5
Coefficient of thermal expansion (10^{-6} °C^{-1})	4.4	2.0
Young's modulus (GPa)	430	110
Tensile strength (MPa)	4100	70

* Manufacturer's specifications.

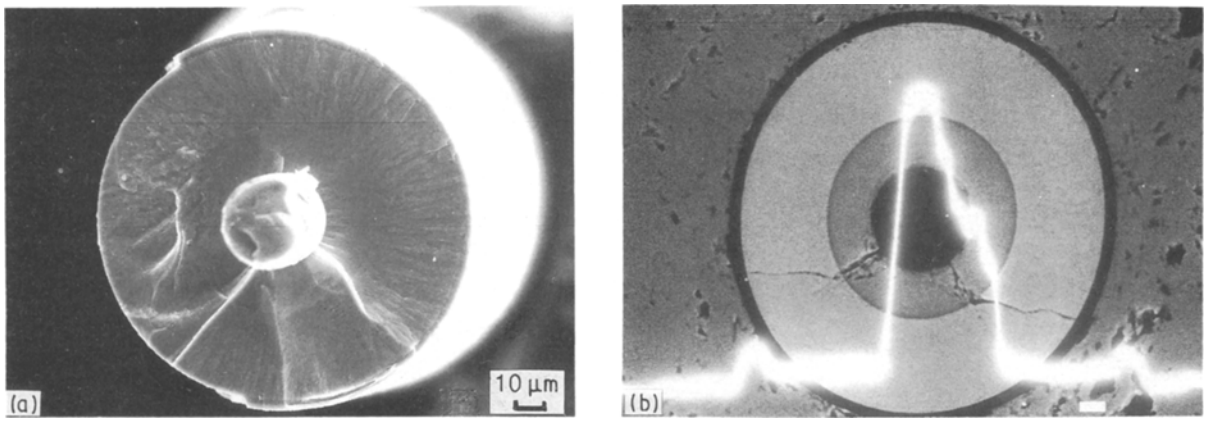

Figure 2 Scanning electron micrograph of the silicon carbide fibre showing (a) fracture surface of the fibre cross-section, and (b) polished cross-section with a superimposed carbon profile.

graphite die was constructed to maintain alignment of the fibre; with this arrangement, the embedded length of the fibre was equal to the thickness of the sample. In order to examine the effect of matrix toughening, samples were fabricated with a matrix of cordierite or cordierite containing 15 vol % SiC whiskers. Additional samples were fabricated in which the fibre was oxidized under controlled conditions prior to incorporation into the matrix. All samples were hot pressed under identical conditions (1050 °C for 25 min under a pressure of 10 MPa) in a high-purity argon atmosphere. The samples were 12 mm in diameter and 1 to 4 mm thick.

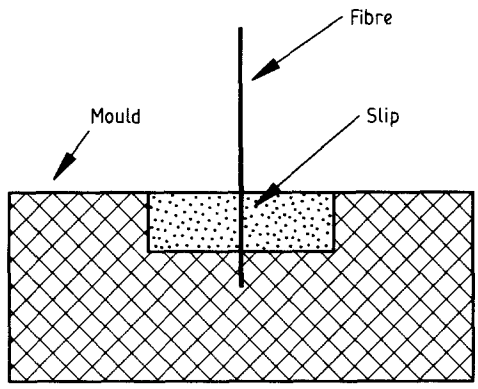

Figure 3 Schematic drawing of the slip-casting method for pull-out test specimens fabricated by conventional sintering.

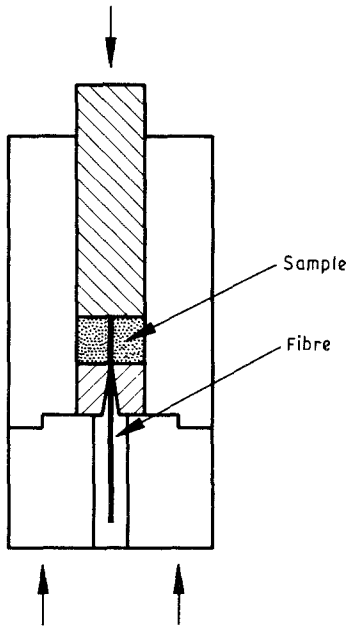

Figure 4 Schematic drawing of the sample preparation method for pull-out test specimens fabricated by hot pressing.

Individual samples were loaded in uniaxial tension on an Instron universal testing machine using a 5 kg load cell. The samples were placed freely on supports that were a fixed distance apart and the fibre was pulled at a rate of 1 mm min^{-1}. The fibre pull-out length was measured from the thickness of the sample and compared with the value measured from the chart speed.

4. Results and discussion

4.1. Theoretical predictions for interface stress

Using the analytical model, the stresses at the interface were determined as a function of the embedded length, l_e, which is also equal to the sample thickness in this work. The shear stress distribution at the fibre matrix interface before debonding occurs (i.e. the elastic interface) is shown in Fig. 5 for three embedded lengths and for a given applied load on the fibre. The shear stress attains its maximum value, τ_{max}, at a finite distance

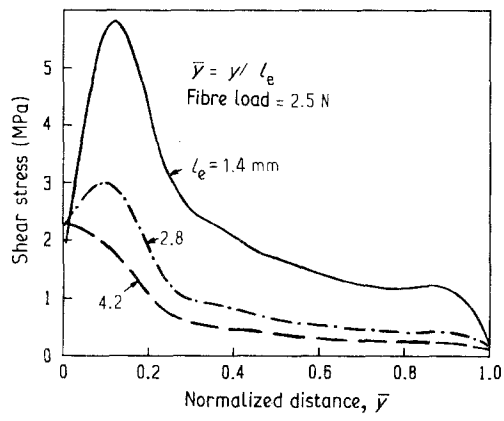

Figure 5 Model predictions of the shear stress distribution at the interface of the sample in the pull-out test.

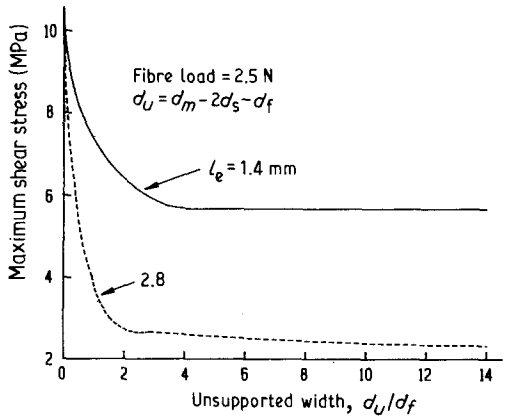

Figure 6 Predicted effect of the support geometry on the maximum shear stress.

from the surface of the sample that is supported on a rigid support. The maximum shear stress depends on the supported length, as shown in Fig. 6 for two typical embedded lengths. For moderately thick samples ($\gtrsim$2.5 mm) the maximum shear stress is less dependent on the support conditions. In addition, for very thin samples the analytical results indicate a large tensile stress at the interface on the pull-out end and a large compressive stress at the corresponding point on the opposite surface of the sample, as shown in Fig. 7. Again, for thicker samples the effect is not significant. It is clear from the present analysis that the sample thickness and the method of supporting the sample need to be carefully controlled during the pull-out test.

4.2. Experimental data from fibre pull-out tests

The single fibre pull-out tests gave data for the load as a function of chart length from which the force–displacement curve was obtained. Fig. 8 shows a typical curve for the samples tested in this work. The force increased linearly with displacement until pull-out began at which point there was a sharp drop in the force. This was followed by a slight increase in the force after which there was further pull-out accompanied by a slight drop in the force. This process continued until the remaining part of the fibre pulled out smoothly. It has been observed by a number of workers and is referred to as "stick–slip" friction [18].

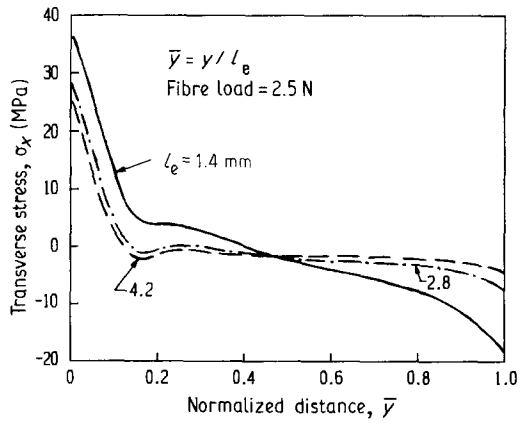

Figure 7 Predicted transverse normal stress distribution at the interface.

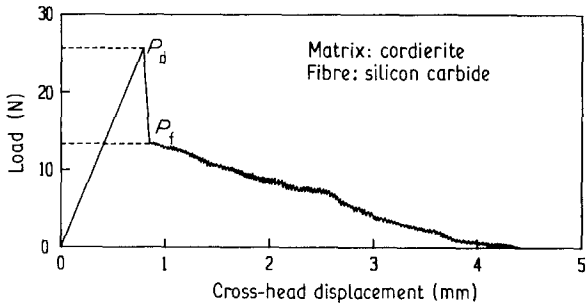

Figure 8 Typical load–displacement curve in the single-fibre pull-out experiment.

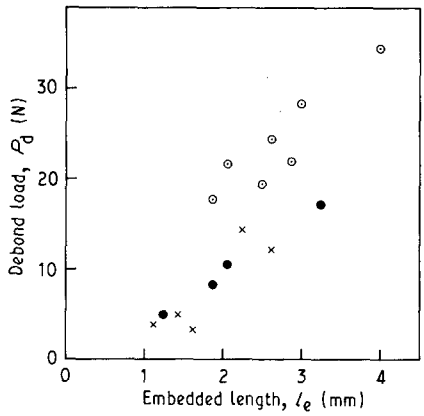

Figure 9 Measured debond load as a function of the fibre embedded length. (○) Sintered, cordierite matrix; (●) hot pressed, cordurite matrix; (×) hot pressed, composite matrix.

As illustrated in Fig. 8, P_d is the maximum force at which pull-out began (referred to as the debond force), and P_f is the force immediately after the sharp drop that followed the initial pull-out (referred to as the frictional force). The debond force as a function of embedded length is shown in Fig. 9 for the sintered and hot-pressed samples; for these samples the fibres were not pretreated prior to incorporation in the matrix and there was no oxidation after the fabrication procedure. The debond force is seen to increase with increasing embedded length. For a fixed embedded length, the debond force for the sintered samples are approximately twice the value for the hot-pressed samples; this can be explained in terms of increased oxidation and chemical bonding for the sintered samples fabricated in air.

4.2.1. Debond stress

If debonding is assumed to occur at the location of the maximum shear stress (i.e. τ_{max}) and when this maximum shear stress reaches the debond stress, τ_d, of the interface, then

$$\tau_d = C\tau_{max}P_d \quad (10)$$

where C is a constant for the sample. The maximum shear stress predicted from the analytical model is shown in Fig. 10 as a function of the embedded length. From the load at the initiation of debonding (measured from the load–displacement curve of the fibre pull-out test) and the maximum shear stress predicted

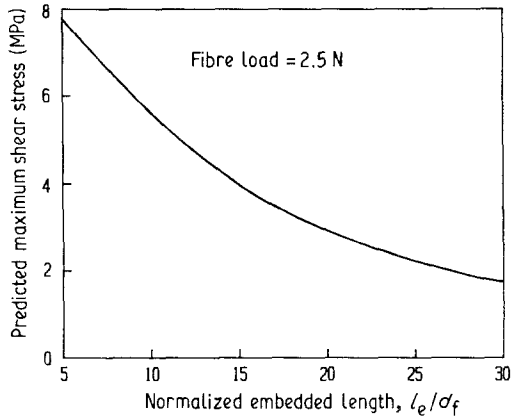

Figure 10. Predicted maximum shear stress at the interface as a function of the normalized embedded length.

by the analytical model for a given embedded length, the debond stress of the interface was calculated from Equation 10 using $C = 0.04$.

The analytical model developed in this paper accounts for the transverse displacements, Poisson's effect, finite length of the sample and the gripping conditions of the sample. The results obtained using the current model will now be compared with the simpler available models. If the shear stress along the interface is assumed constant the average and the maximum shear stresses will be equal. Further, they are equal to the debond stress of the interface at the initiation of debonding [19], so that

$$\tau_d = P_d/2\pi r_f l_e \quad (11)$$

where r_f and l_e are the radius and the embedded length of the fibre, respectively. The assumption of uniform shear stress along the interface is realistic only for very short embedded lengths and for matrices that yield readily. The variation of shear stress along the interface for elastic–elastic systems has been modelled [1, 2] using classical shear-lag assumptions. According to these models the maximum shear stress occurs at the point where the fibre enters the matrix. Again, by assuming that at the onset of debonding the maximum shear stress and debond stress are equal, the debond stress can be represented by the following two-parameter relationship [10]

$$P_d = A\tanh(\alpha l_e) \quad (12)$$

where

$$A = \tau_d 2\pi r_f/\alpha \quad (13)$$

and α is a parameter that depends on the shear modulus of the matrix, the Young's modulus of the fibre and radii of the fibre and the matrix. A non-linear regression was carried out to find the best fit through P_d–l_e data for a given material system and hence determine A and α. Knowing these two constants, τ_d can be calculated. The debond stresses calculated using Equations 10 to 12 and experimental pull-out loads are given in Table II.

4.2.2. Frictional stress

Once the debonding is completed, the fibre is pulled out gradually against frictional resistance. This frictional stress (τ_f) is constant along the interface and can be calculated knowing the frictional load, P_f, from the pull-out test by

$$\tau_f = P_f/2\pi r_f l_e \quad (14)$$

The frictional stresses (τ_f) calculated using Equation 14 for various interface conditions are listed in Table III. The results for the samples with a composite matrix (cordierite/15 vol % whiskers) are not significantly different from those for the unreinforced cordierite matrix. An important observation, however, is the drastic effect of processing conditions and oxidation on the interfacial properties.

TABLE II Experimental data for the debond stress τ_d

Sample description	τ_d (MPa)		
	Eq. 11	Eq. 10	Eq. 12
1. Hot-pressed samples:			
(a) cordierite matrix/untreated fibre	11	15	12
(b) cordierite matrix/oxidized fibre	17	24	25
(c) composite matrix/untreated fibre	9	13	11
(d) composite matrix/oxidized fibre	13	15	13
2. Sintered samples:			
(a) 950 °C, 2.5 h, air	21	30	33
(b) 950 °C, 2.5 h, and 1050 °C, 2 h, air	32	51	37

TABLE III Experimental data for frictional stress, τ_f

Sample description	τ_f (MPa)
1. Hot-pressed samples:	
(a) cordierite matrix/untreated fibre	5
(b) cordierite matrix/oxidized fibre	8
(c) composite matrix/untreated fibre	6
(d) composite matrix/oxidized fibre	8
2. Sintered samples:	
(a) 950 °C, 2.5 h, air	8
(b) 950 °C, 2.5 h, and 1050 °C, 2 h, air	23

5. Conclusions

An analytical model based on a consistent shear-lag theory showed that the sample thickness and the support conditions during testing must be carefully controlled in the single fibre pull-out test.

For single SiC fibres embedded in a cordierite matrix, the measured interfacial debond stress was 11 MPa for samples fabricated by hot pressing in high-purity argon. Processing in air or oxidation produced a significant increase in the debond stress and the interfacial frictional stress.

For a fixed support condition, various models agree in trend but predict different stresses at debonding using the same test data.

References

1. L. B. GRESZCZUK. in "Interfaces in Composites", ASTM STP 452 (American Society for Testing and Materials, Philadelphia, Pennsylvania, 1969) pp. 42–58.
2. P. J. LAWRENCE. *J. Mater. Sci.* 7 (1972) 1.

3. A. TAKAKU and R. G. C. ARRIDGE, *J. Phys. D Appl. Phys.* **6** (1973) 2038.
4. B. HARRIS, J. MORLEY and D. C. PHILLIPS, *J. Mater. Sci.* **10** (1975) 2050.
5. P. BARTOS, *ibid.* **15** (1980) 3122.
6. R. J. GRAY, *ibid.* **19** (1984) 861.
7. P. S. CHUA and M. R. PIGGOTT, *Compos. Sci. Technol.* **22** (1985) 33.
8. U. V. DESHMUKH and T. W. COYLE, *Ceram. Engng Sci. Proc.* **9** (1988) 627.
9. R. W. GOETTLER and K. T. FABER, *ibid.* **9** (1988) 861.
10. *Idem, Compos. Sci. Technol.* **37** (1989) 129.
11. C. W. GRIFFIN, S. Y. LIMAYE, D. W. RICHERSON and D. K. SHETTY, *Ceram. Engng. Sci. Proc.* **9** (1988) 671.
12. D. B. MARSHALL and A. G. EVANS, *J. Amer. Ceram. Soc.* **68** (1985) 225.
13. D. B. MARSHALL, *ibid.* **67** (1984) C-259.
14. D. B. MARSHALL and W. C. OLIVER, *ibid.* **70** (1987) 542.
15. L. R. DHARANI, Final Report, NSF Grant no. 8504591 (1988).
16. L. R. DHARANI and H. TANG, *Int. J. Fract.* (1989) in press.
17. "Ceramic Source", Vol. 2 edited by L. Kefron (American Ceramic Society, 1986).
18. P. S. CHUA and M. R. PIGGOTT, *Compos. Sci. Technol.* **22** (1985) 107.
19. F. J. McGARRY and D. W. MARSHALL, in "Symposium on Standards for Filament-Wound Reinforced Plastics", ASTM STP 327 (American Society for Testing and Materials, Philadelphia, Pennsylvania, 1963) pp. 133–45.

Received 16 October 1989
and accepted 20 March 1990